

Electronic Supplementary Information (ESI) Section

Experimental and Theoretical Study of Aqueous *Cis*-Pinonic Acid Photolysis

Hanna Lignell^{1,2}, Scott A. Epstein¹, Margaret R. Marvin¹, Dorit Shemesh³, Benny Gerber^{1,2,3},
Sergey Nizkorodov^{1,*}

¹ *Department of Chemistry, University of California, Irvine, CA 92697-2025, USA*

² *Laboratory of Physical Chemistry, P.O. Box 55, FIN-00014 University of Helsinki, Finland*

³ *Institute of Chemistry and The Fritz Haber Research Center, The Hebrew University,
Jerusalem 91904, Israel*

* Corresponding author: nizkorod@uci.edu, 1-949-824-1262

Contents

List of Abbreviations Used in This Work.....	2
Aqueous Photolysis Experiments.....	3
Absorption Cross Sections and Molar Extinction Coefficients of Aqueous <i>Cis</i> -Pinonic Acid	4
Actinometer Used in Aqueous Photolysis Measurements	7
Analysis of Broadband-UV Aqueous Photolysis Data	7
HPLC Separation of PA Photolysis Products and Fraction Collection.....	12
Gas-Phase Photolysis Experiments and Data Analysis.....	13
NMR Shifts for PA and Its Isomer (Limononic Acid).....	15
Kinetics of Aqueous-Phase Photolysis of PA	17
Gas-Phase Quantum Yield Measurements Relative to Acetone	20
Gas-Phase PAMe Photolysis Products with the PTR-ToF-MS	20
Supporting Information for the Computational Section.....	23

List of Abbreviations Used in This Work

BVOC:	Biogenic Volatile Organic Compound(s)
CC2:	Second-Order Approximate Coupled-Cluster (method)
ESI:	Electronic Supporting Information or Electro-Spray Ionization, depending on the context
FWHM:	Full Width at Half-Maximum
GC-CIMS:	Gas Chromatography - Chemical Ionization Mass Spectroscopy
HPLC:	High-Performance Liquid Chromatography
ISC:	InterSystem Crossing
LWC:	Liquid Water Content
MNDO:	Modified Neglect of Diatomic Overlap
MP2:	Møller-Plesset (perturbation theory)
MRCI:	Multi-Reference Configuration Interaction
NMR:	Nuclear Magnetic Resonance
OM2:	Orthogonalization-corrected Method 2
PA:	<i>cis</i> -Pinonic Acid
PAMe:	<i>cis</i> -Pinonic Acid Methyl ester
PDA:	PhotoDiode Array (spectrometer)
PM3:	Parameterized Model number 3
PTR-ToF-MS	Proton-Transfer-Reaction Time-of-Flight Mass Spectrometer
RI:	Resolution-of-Identity (approximation)
SIMPOL:	Simplified P_L^0 prediction method (from Pankow, J. F. and Asher, W. E.: SIMPOL.1: a simple group contribution method for predicting vapor pressures and enthalpies of vaporization of multifunctional organic compounds, <i>Atmos. Chem. Phys.</i> , 8, 2773-2796, doi:10.5194/acp-8-2773-2008, 2008)
SOA:	Secondary Organic Aerosol
SZA:	Solar Zenith Angle
TMS:	TetraMethylSilane
UV-Vis:	Ultraviolet-Visible (absorption spectroscopy)
WSOC:	Water Soluble Organic Compound(s)

Aqueous Photolysis Experiments

This study relies on broadband photolysis of aqueous solutions of *cis*-pinonic acid (abbreviated as PA below) in standard 10 mm quartz cuvettes. The layout of the experimental setup is shown in Figure S1, and the spectral distribution of the radiation entering the cuvette is shown in Figure S2.

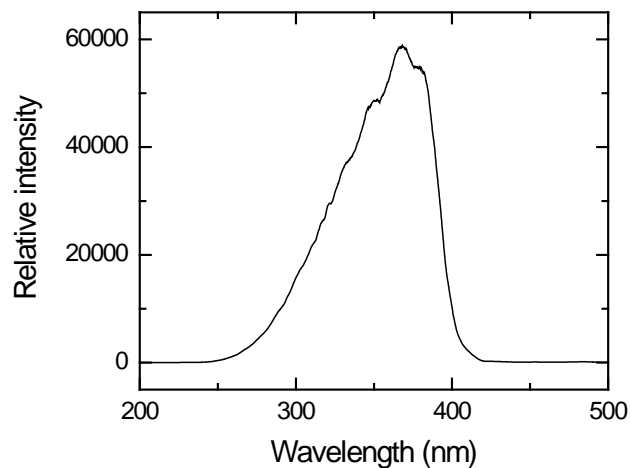
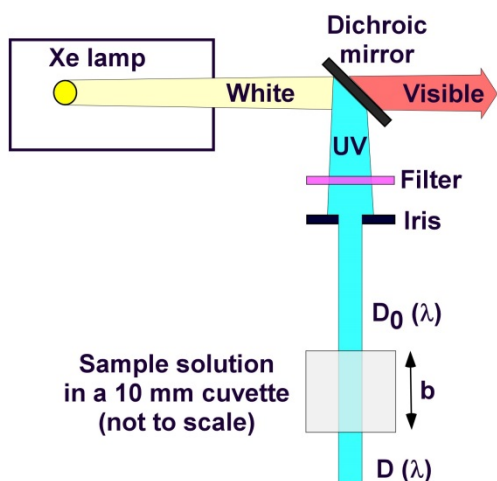


Figure S1. Schematic layout of the experimental setup for aqueous phase photolysis (top view). The dichroic mirror (Newport model 60159) serves to isolate the 280-400 nm band, and the U330 filter further limits the transmission of the visible and near-IR radiation.

Figure S2. The spectrum of the radiation used in the aqueous photolysis experiments recorded with an Ocean Optics USB4000 spectrometer. The shape of the spectrum will be referred to as $OO(\lambda)$ in the derivations below.

Absorption Cross Sections and Molar Extinction Coefficients of Aqueous *Cis*-Pinonic Acid

In order to determine the quantum yield of PA photolysis, molar extinction coefficients of PA in water were required. Since they have not been published previously, we determined them in this study. Figure S3 shows the Beer-Lambert plot measured at the peak of the $\pi^* \leftarrow n$ transition of PA and a series of absorption spectra recorded at different concentrations of PA. We report base-e absorption cross sections in Fig. S3 and also list them in Table S1 along with the base-10 molar extinction coefficients.

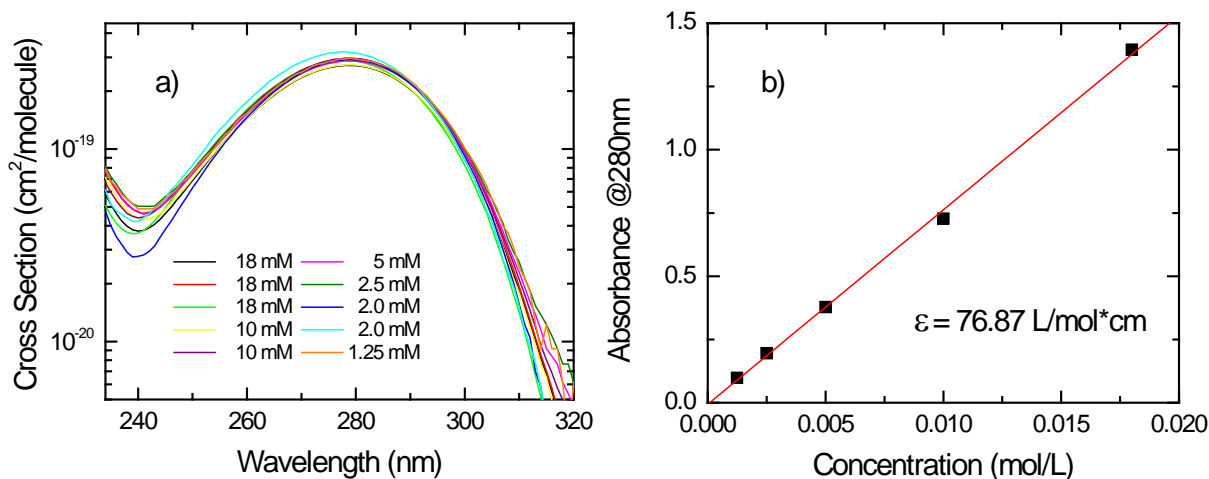


Figure S3. a) Absorption cross sections of PA in water obtained at concentrations varying from 1.25 mM to 18 mM. b) A representative Beer-Lambert plot for PA in water at the peak of the $\pi^* \leftarrow n$ band.

Table S1. Decadal (base-10) extinction coefficients and base-e absorption cross sections of PA in water obtained by averaging 10 data sets with concentrations shown in Fig. S3.

Wavelength (nm)	Base-10 extinction coefficient (1/M*cm)	Standard deviation of extinction coefficient	Base-e absorption cross section (cm ² /molecule)
234	17.53	3.18	6.70E-20
235	15.35	2.86	5.87E-20
236	13.95	2.72	5.33E-20
237	12.77	2.38	4.88E-20
238	11.96	2.21	4.57E-20
239	11.39	2.03	4.35E-20
240	11.12	1.81	4.25E-20
241	11.17	1.71	4.27E-20
242	11.40	1.62	4.36E-20
243	11.80	1.53	4.51E-20
244	12.46	1.46	4.77E-20
245	13.31	1.43	5.09E-20
246	14.28	1.45	5.46E-20
247	15.30	1.38	5.85E-20
248	16.59	1.43	6.34E-20
249	17.86	1.43	6.83E-20
250	19.34	1.43	7.39E-20
251	21.02	1.53	8.04E-20
252	22.74	1.59	8.69E-20
253	24.63	1.70	9.42E-20
254	26.61	1.86	1.02E-19
255	28.75	1.99	1.10E-19
256	30.91	1.94	1.18E-19
257	33.07	2.19	1.26E-19
258	35.62	2.22	1.36E-19
259	38.05	2.39	1.45E-19
260	40.46	2.46	1.55E-19
261	43.12	2.59	1.65E-19
262	45.70	2.73	1.75E-19
263	48.36	2.86	1.85E-19
264	51.07	3.13	1.95E-19
265	53.74	3.11	2.05E-19
266	56.42	3.23	2.16E-19
267	58.88	3.26	2.25E-19
268	61.45	3.42	2.35E-19
269	63.81	3.49	2.44E-19
270	65.97	3.46	2.52E-19
271	68.01	3.47	2.60E-19
272	69.89	3.55	2.67E-19
273	71.54	3.51	2.74E-19
274	72.88	3.57	2.79E-19
275	74.15	3.66	2.84E-19
276	74.99	3.56	2.87E-19
277	75.77	3.55	2.90E-19
278	76.13	3.55	2.91E-19
279	76.18	3.34	2.91E-19
280	75.80	3.25	2.90E-19
281	75.15	3.17	2.87E-19
282	74.21	3.01	2.84E-19

283	73.07	2.98	2.79E-19
284	71.43	2.76	2.73E-19
285	69.64	2.72	2.66E-19
286	67.55	2.66	2.58E-19
287	65.25	2.58	2.49E-19
288	62.63	2.43	2.39E-19
289	59.81	2.33	2.29E-19
290	56.83	2.27	2.17E-19
291	53.74	2.23	2.05E-19
292	50.34	2.05	1.92E-19
293	47.07	2.08	1.80E-19
294	43.58	1.99	1.67E-19
295	40.13	1.96	1.53E-19
296	36.77	1.93	1.41E-19
297	33.55	1.86	1.28E-19
298	30.34	1.74	1.16E-19
299	27.25	1.74	1.04E-19
300	24.29	1.59	9.29E-20
301	21.64	1.61	8.27E-20
302	19.06	1.63	7.29E-20
303	16.61	1.59	6.35E-20
304	14.34	1.49	5.48E-20
305	12.40	1.42	4.74E-20
306	10.48	1.44	4.01E-20
307	8.74	1.33	3.34E-20
308	7.37	1.26	2.82E-20
309	6.14	1.14	2.35E-20
310	5.11	1.05	1.95E-20
311	4.19	1.00	1.60E-20
312	3.48	0.90	1.33E-20
313	2.73	0.76	1.04E-20
314	2.22	0.71	8.50E-21
315	1.92	0.83	7.33E-21
316	1.57	0.73	6.01E-21
317	1.24	0.85	4.73E-21
318	0.97	0.67	3.71E-21
319	0.77	0.62	2.94E-21
320	0.70	0.62	2.67E-21
321	0.50	0.46	1.89E-21
322	0.48	0.56	1.85E-21
323	0.37	0.50	1.43E-21
324	0.34	0.52	1.31E-21
325	0.18	0.49	6.76E-22
326	0.11	0.39	4.39E-22
327	0.11	0.34	4.25E-22
328	0.12	0.41	4.50E-22
329	0.20	0.56	7.65E-22
330	0.14	0.47	5.20E-22

Actinometer Used in Aqueous Photolysis Measurements

We rely on chemical actinometry to determine the amount of radiation passing through the cuvette. We used azoxybenzene as an actinometer {Bunce, 1984 #221} because its photoisomerization quantum yield is relatively independent of temperature and concentration over the wavelength range of interest. Azoxybenzene efficiently photoisomerizes as follows, with $\phi_{act} = 0.021 \pm 0.0019$ (the average value of the 22°C experiments reported by Bunce *et al.* (1984)).

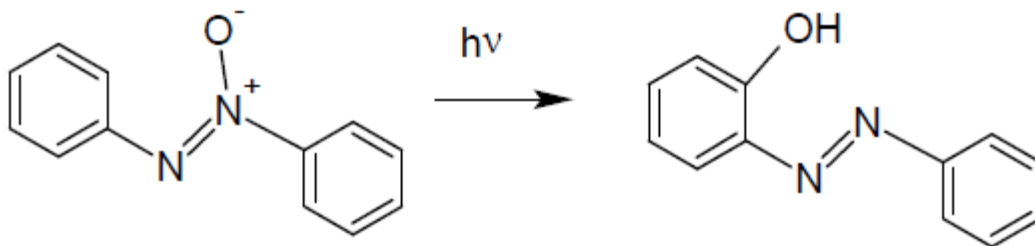


Figure S4: Photoisomerization of azoxybenzene.

Analysis of Broadband-UV Aqueous Photolysis Data

The quantum yield ϕ_{PA} for the photolysis of aqueous PA is determined by photolyzing a solution of PA and a solution of actinometer under identical irradiation conditions. As we expect to carry out related experiments in the future, we are going to describe the measurement and data analysis procedure in some detail. It is convenient to define the following parameters:

- $D(\lambda)$ (photons $\text{cm}^{-2} \text{s}^{-1} \text{nm}^{-1}$) – spectral flux density of radiation. This represents the number of photons crossing a unit area per second per wavelength interval. In laboratory experiments, all photons generally travel in approximately the same direction from the light source; therefore, solid angle dependence is not considered.
- F (photons $\text{cm}^{-2} \text{s}^{-1}$) – spectral flux of radiation. This represents the number of photons crossing a unit area per second, integrated over the wavelength range of interest. In the experiments described in the main text, the wavelength range is 280-400 nm, although some visible colors may contribute if the light is not filtered sufficiently well.

$$F = \int_{\lambda} D(\lambda) d\lambda \quad (\text{S1})$$

- **Area** (cm^2) – beam area. The flux is assumed to be uniform across this area and drop to zero outside this area. The area in this experiment was defined by an iris placed in front of the sample (see Figure S1).
- ***b*** (cm) – physical path length through the sample. Since the cuvette is irradiated from a side, *b* is equal to the cuvette width (1 cm). (In a limited number of experiments, the cuvette was irradiated from the top, in which case *b* was equal to the height of the solution in the cuvette).

- V_{liquid} (cm^3) – sample volume, typically 3-4 cm^3 in these experiments.
- $V_{irradiated}$ (cm^3) – the volume swept by the light beam inside the cuvette, typically $\sim 1 \text{ cm}^3$ in these experiments. Note that we use this definition regardless of the optical density of the solution, as if all incoming radiation is coming through the cuvette without attenuation. We also neglect photolysis by the radiation scattered off the cuvette walls. Therefore:

$$V_{irradiated} = Area \times b \quad (\text{S2})$$

- $f_{irradiated}$ – the fraction of the solution volume situated in the direct path of the radiation.

$$f_{irradiated} = \frac{V_{irradiated}}{V_{liquid}} = \frac{Area \times b}{V_{liquid}} \quad (\text{S3})$$

- I (photons s^{-1}) – intensity of radiation or rate with which photons are supplied to the sample. This represents the number of photons entering (subscript "0" will be attached in this case) or exiting the sample per second, integrated over the wavelength of interest and beam area.

$$I = Area \times F \quad (\text{S4})$$

- n (molecules cm^{-3}) – number concentration of molecules in the solution. Although it is not common to use this concentration unit for liquid-phase measurements, the derivations are more straightforward with the molecule base units.
- C (mol L^{-1}) – molar concentration of molecules in the sample, the usual metric for solution concentrations. This can be easily converted to the units of n (molecule cm^{-3}) as follows (N_A is the Avogadro constant):

$$C = 1000 \left(\frac{\text{cm}^3}{\text{L}} \right) \times \frac{n}{N_A} \quad (\text{S5})$$

- k (molecule s^{-1}) – the apparent first-order rate constant for the photolysis (known as photolysis rate constant, J , in atmospheric photochemistry). Its value does not depend on which concentration units are used.

$$\begin{aligned} -\frac{dC}{dt} = k \times C & \quad \text{or} \quad k = -\frac{1}{C} \frac{dC}{dt} \\ -\frac{dn}{dt} = k \times n & \quad \text{or} \quad k = -\frac{1}{n} \frac{dn}{dt} \end{aligned} \quad (\text{S6})$$

- $\phi(\lambda)$ (molecule photon $^{-1}$) – wavelength-dependent quantum yield for photolysis. In this work, we are measuring the *effective wavelength-averaged quantum yield*, $\langle \phi_x \rangle$, averaged over the wavelength range of photolysis radiation, as described below.
- $\alpha(\lambda)$ ($\text{cm}^2 \text{ molecule}^{-1}$) – base-e absorption cross section. This is a measure of optical absorption typically used in gas-phase absorption spectroscopy. For PA, the relevant cross sections are listed in Table S1 and shown in Figure S3.

- $\epsilon(\lambda)$ ($\text{L mol}^{-1} \text{cm}^{-1}$) – base-10 molar absorptivity, a.k.a., molar extinction coefficient. This quantity is normally used in liquid-phase spectroscopy. It is related to the absorption cross section through the following formula:

$$\epsilon(\lambda) = \sigma(\lambda) \times \frac{N_A}{1000 \times \ln(10)} \quad (\text{S7})$$

Note that the conversion factor of 1000 only works for the default units specified above.

- $A_e(\lambda)$ – base-e absorbance through the sample, which in the absence of other absorbers and scatterers is equal to:

$$A_e(\lambda) = \sigma(\lambda) \times n \times b \quad (\text{S8})$$

- $A_{10}(\lambda)$ – base-10 absorbance through the sample. This is the quantity returned by commercial UV-Vis and FTIR spectrometers.

$$A_{10}(\lambda) = \epsilon(\lambda) \times C \times b = \frac{A_e(\lambda)}{\ln(10)} \quad (\text{S9})$$

The relative spectral density, $OO(\lambda)$, of the radiation entering the solution was measured with an Ocean Optics spectrometer (see Figure S2). We corrected for the reflection/transmission losses from the front window of the cuvette by measuring $OO(\lambda)$ before and after the cuvette filled with blank solution and taking the average (for details, see the classical book “Photochemistry” by Calvert and Pitts, 1966). The function $OO(\lambda)$ is dimensionless and it can be arbitrarily scaled. We assume that the actual spectral flux density of radiation entering the solution is directly proportional to $OO(\lambda)$:

$$D_0(\lambda) = \alpha \times OO(\lambda) \quad (\text{S10})$$

where α is a scaling constant that contains all the units associated with $D_0(\lambda)$. The actinometer makes it possible to determine the value of α for each specific experimental configuration.

Only a fraction of the incoming radiation will be accessible to photochemistry, with the remainder passing through the cuvette. From the Beer-Lambert law, the fraction of the absorbed radiation at a given wavelength is:

$$\frac{D(\lambda)}{D_0(\lambda)} = e^{-A_e(\lambda)} = e^{-\sigma(\lambda) \times n \times b} \quad (\text{S11})$$

It can be shown that the broadband photolysis rate for the dissolved compound X (= actinometer or PA) in the limit of rapid mixing within the cuvette can be represented as follows:

$$-\frac{dn_X}{dt} = \frac{f_{\text{irradiated}}}{b} \times \int_{\lambda} D_0(\lambda) \left[1 - e^{-\sigma_X(\lambda) \times n_X \times b} \right] \phi_X(\lambda) d\lambda \quad (\text{S12})$$

As already pointed out above, our experiment measures the effective wavelength-averaged quantum yield, $\langle \phi_X \rangle$, defined as follows:

$$-\frac{dn_X}{dt} = \langle \phi_X \rangle \times \frac{f_{irradiated}}{b} \times \int_{\lambda} D_0(\lambda) \left[1 - e^{-\sigma_X(\lambda) \times n_X \times b} \right] d\lambda \quad (S13)$$

Note that the above equation does not describe the first-order loss of X. The rate is not directly proportional to the concentration because of the exponential term in the equation. Furthermore, the rate changes with the photolysis time in a non-linear way as X is slowly depleted by the photolysis. To avoid non-linear fitting of data, we use equation S13 in the limit of small photolysis times, when compound X is not yet appreciably depleted by photolysis, i.e., $n_X(t) \sim n_X(t=0)$.

In the limit of an optically thin solution ($A_e(\lambda) \ll 1$ at all wavelengths of interest), equation S13 simplifies to the normal first-order loss, where k is the effective first-order loss constant (equation S6):

$$-\frac{dn_X}{dt} = \langle \phi_X \rangle \times f_{irradiated} \times n_X \times \int_{\lambda} D_0(\lambda) \sigma_X(\lambda) d\lambda = k \times n_X \quad (S14)$$

$$k = \langle \phi_X \rangle \times f_{irradiated} \times \int_{\lambda} D_0(\lambda) \sigma_X(\lambda) d\lambda \quad (S15)$$

Conversely, in the limit of an optically thick solution ($A_e(\lambda) \gg 1$ at all wavelengths of interest), the rate becomes independent of photolysis time and concentration (because every incoming photon is absorbed by the solution). Therefore, photolysis in this case is effectively a zero-order process:

$$-\frac{dn_X}{dt} = \frac{f_{irradiated}}{b} \times \langle \phi_X \rangle \times \int_{\lambda} D_0(\lambda) d\lambda = \frac{f_{irradiated}}{b} \times \langle \phi_X \rangle \times F_0 = \frac{I_0 \times \langle \phi_X \rangle}{V_{liquid}} \quad (S16)$$

In the experiments described in this paper, the photolysis of an actinometer solution was carried out under conditions approaching the optically-thick limit, whereas photolysis of PA was carried out under conditions approaching the optically-thin limit. However, we used the general equation S13 in both cases, and carried out the numeric integration over wavelength using Mathematica. Briefly, the radiation flux was first calibrated by experimentally determining the rate of photolysis of the actinometer and calculating the parameter α in the limit of small photolysis times from the following equations:

$$\alpha = \frac{\left(-\frac{dn_{act}}{dt} \right) \times \frac{b}{\langle \phi_{act} \rangle f_{irradiated}}}{\int_{\lambda} D_0(\lambda) \left[1 - e^{-\sigma_{act}(\lambda) \times n_{act} \times b} \right] d\lambda} \quad (S17)$$

After the spectral flux density is calibrated with the actinometer, the quantum yield of PA photolysis, ϕ_{PA} , can be calculated using a similarly derived equation:

$$\langle \phi_{PA} \rangle = \frac{\left(-\frac{dn_{PA}}{dt} \right) \times \frac{b}{\alpha f_{irradiated}}}{\int_{\lambda} D_0(\lambda) \left[1 - e^{-\sigma_{PA}(\lambda) \times n_{PA} \times b} \right] d\lambda} \quad (S18)$$

The rate of loss of actinometer and PA loss were determined as described in the main text. Note that the exact knowledge of the irradiated fraction is not required in these experiments as it is going to cancel out from combining equations S17 and S18 above:

$$\langle \phi_{PA} \rangle = \langle \phi_{act} \rangle \times \frac{\left(-\frac{dn_{PA}}{dt} \right) \int OO(\lambda) \left[1 - e^{-\sigma_{act}(\lambda) \times n_{act} \times b} \right] d\lambda}{\left(-\frac{dn_{act}}{dt} \right) \int_{\lambda} OO(\lambda) \left[1 - e^{-\sigma_{PA}(\lambda) \times n_{PA} \times b} \right] d\lambda} \quad (\text{S19})$$

Equation S19 was used in all quantum yield calculations described in this paper. The slopes entering equation S19 were obtained from experiments.

HPLC Separation of PA Photolysis Products and Fraction Collection

We carried out numerous HPLC separations of the aqueous PA photolysis products using both photodiode array (PDA) and electrospray mass spectrometry (ESI-MS) detectors. Figure S5 shows a typical result using the Shimadzu SPD-10Avp (200-650 nm spectral range) PDA detector. The two strongest peaks observed in the 261 nm chromatogram at 30.5 min and 32.0 min correspond to PA and its photoisomer, limonic acid (see Scheme 1 in the manuscript), respectively. Both compounds retain the carbonyl group as confirmed by the presence of a distinct 280 nm absorption band in the absorption spectrum. The remaining peaks correspond to less significant photolysis products.

For collection of fractions, the PDA signal was observed in real time, and the eluent from the PDA detector was sent into a scintillation vial when the peak of interest started to appear. The collection stopped when the peak nearly decayed back to the baseline. Because each collected fraction did not have enough material for NMR analysis, the collection was repeated several times, as mentioned in the manuscript.

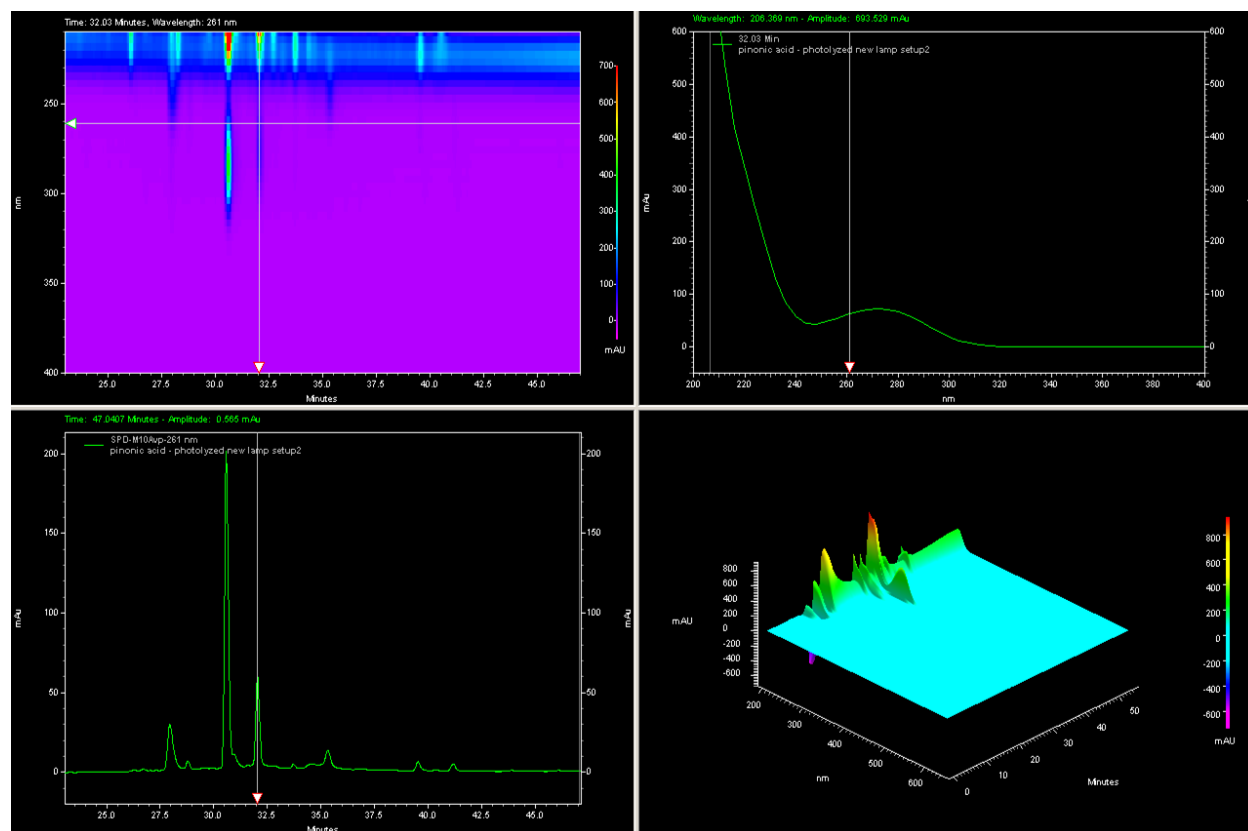


Figure S5. A sample HPLC-PDA experiment. The top-left corner shows a two-dimensional view of the HPLC-PDA data. The bottom-left corner shows a horizontal cut through this data set, corresponding to a chromatogram recorded by monitoring the 261 nm absorbance. The top-right corner shows a vertical cut at 32 min, corresponding to the absorption spectrum of the PA isomer.

Gas-Phase Photolysis Experiments and Data Analysis

The layout of the experimental setup for gas-phase photolysis of PA methyl ester (PAMe) is shown in Fig. S6, and the spectral distribution of the radiation entering the Teflon chamber is shown in Fig. S7.

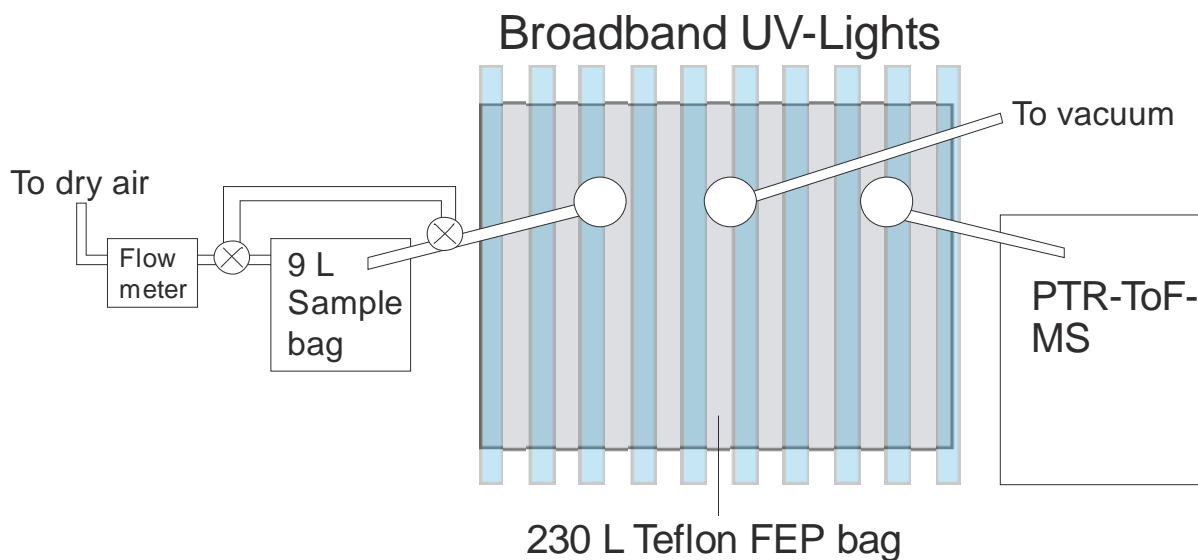


Figure S6. A schematic diagram of the gas-phase photolysis setup. The vertical bars behind the Teflon bag represent a bank of UV-B lamps (Philips, TL 40W/12 RS). The intermediate 9 L bag is used to prevent injecting any liquid into the main bag.

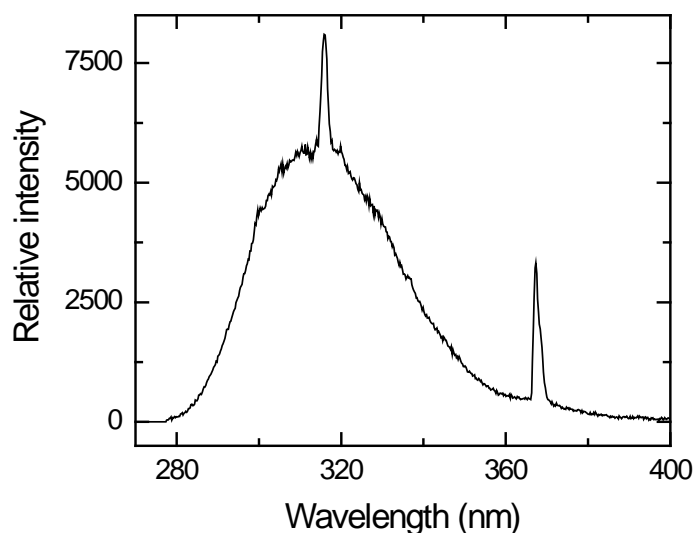


Figure S7. The spectrum of the radiation used in the gas-phase photolysis experiments recorded with an Ocean Optics USB4000 spectrometer in front of the Teflon bag. The shape of the spectrum will be referred as $OO(\lambda)$ in the derivations.

The analysis of the gas-phase photolysis experiments is similar to that of liquid-phase photolysis experiments with the following important distinctions:

1. The concentrations are small, and therefore the optically-thin limit applies.
2. We use gas-phase acetone as an actinometer and explicitly account for the wavelength dependence of its photolysis quantum yield (taken from the NASA JPL “Chemical Kinetics and Photochemical Data for Use in Atmospheric Studies” evaluation, 2011 edition).

The appropriate equations for the photolysis rate of the actinometer and PA ester become (we assume that $f_{irradiated} = 1$):

$$-\frac{dn_{acetone}}{dt} = n_{acetone} \times \int_{\lambda} D_0(\lambda) \sigma_{acetone}(\lambda) \phi_{acetone}(\lambda) d\lambda \quad (S20)$$

$$-\frac{dn_{PA}}{dt} = n_{PA} \times \langle \phi_{PA} \rangle \times \int_{\lambda} D_0(\lambda) \sigma_{PA}(\lambda) d\lambda \quad (S21)$$

Using the assumption (equation S10) that the spectral flux density is directly proportional to the measured emission spectrum from the lamps (Figure S4), and eliminating the scaling parameter α from the equations, we arrive at:

$$\langle \phi_{PA} \rangle = \frac{k_{PA}}{k_{acetone}} \times \frac{\int_{\lambda} I(\lambda) \sigma_{acetone}(\lambda) \phi_{acetone}(\lambda) d\lambda}{\int_{\lambda} I(\lambda) \sigma_{PA}(\lambda) d\lambda} \quad (S22)$$

where the first-order rate constants are obtained by fitting the PTR-MS data to an exponential loss function (refer to Figure S9 below for the examples of such fits):

$$k_{PA} = -\frac{1}{n_{PA}} \frac{dn_{PA}}{dt} \quad k_{acetone} = -\frac{1}{n_{acetone}} \frac{dn_{acetone}}{dt} \quad (S23)$$

NMR Shifts for PA and Its Isomer (Limononic Acid)

Table S3. Carbon-13 (C13) and proton (H1) NMR data determined in this work. Note that the NMR peak positions for the PA isomer, 3-isopropenyl-6-oxoheptanoic acid (a.k.a., limononic acid, CAS 4436-82-2) are reported here for the first time to the best of our knowledge. All shifts are specified in ppm with respect to TMS reference.

PA C13 exp [*] in CD ₃ CN	PA C13 exp ^a in CDCl ₃	PA C13 exp [*] in CDCl ₃	PA C13 exp ^b in CDCl ₃	PA C13 calc ^c	PA H1 exp [*] in CD ₃ CN	PA H1 exp [*] in CDCl ₃	PA H1 exp ^b in CDCl ₃	PA isomer C13 exp [*] in CDCl ₃	PA isomer calc ^c	PA isomer H1 exp [*] in CDCl ₃	PA isomer H1 calc ^b
207.26	207.8	207.59	207.55	206.46	-	-	11 (1 H)	211.69	208.33	4.88 (S)	4.84 (S)
173.33	177.5	178.02	178.65	172.5	2.93-2.99 (M)	2.93-2.97 (M)	2.894 (M, 1H)	184.4	179.16	4.83 (S)	4.77 (S)
53.7	54	54.25	54.32	56.67	2.31-2.38 (M)	2.39-2.44 (M)	2.38 (M, 1H)	145.24	146.87	2.58-2.66 (M)	2.63-2.72 (M)
42.76	43.1	43.3	43.33	45.2	2.23-2.27 (M)	2.35-2.37 (M)	2.32 (M, 2H)	113.14	112.5	2.43-2.51 (M)	2.47-2.53 (M)
37.75	37.6	37.75	37.89	39.58	2.02 (S)	2.11 (S)	2.055 (S, 3H)	42.89	42.7	2.23-2.35 (M)	2.27-2.34 (M)
34.19	34.7	34.72	34.87	35.42	1.997-2.003 (M)	2.06-2.08 (M)	1.99 (M, 1H)	41.18	41.25	2.19 (S)	2.09 (S)
29.38	29.9	30.27	30.27	30.2	1.87-1.93	1.99-2.04 (M)	1.96 (M, 1H)	38.69	34.38	1.76-1.86 (M)	1.78-1.88 (M)
29.27	29.9	-	30.12	-	1.34 (S)	1.40 (S)	1.333 (S, 3H)	30.12	29.79	1.71 (S)	1.70 (S)
22.83	22.9	23.03	23.2	27.08	0.86 (S)	0.94 (S)	0.878 (S, 3H)	26.23	28.33	1.64-1.70 (M)	1.56-1.66 (M)
17.38	17	17.39	17.35	20.83				18.48	19.79		

^a AIST: Integrated Spectral Database System of Organic Compounds. (Data were obtained from the National Institute of Advanced Industrial Science and Technology (Japan))

^b Predicted NMR data calculated using Advanced Chemistry Development, Inc. (ACD/Labs) Software V11.01 (© 1994-2013 ACD/Labs)

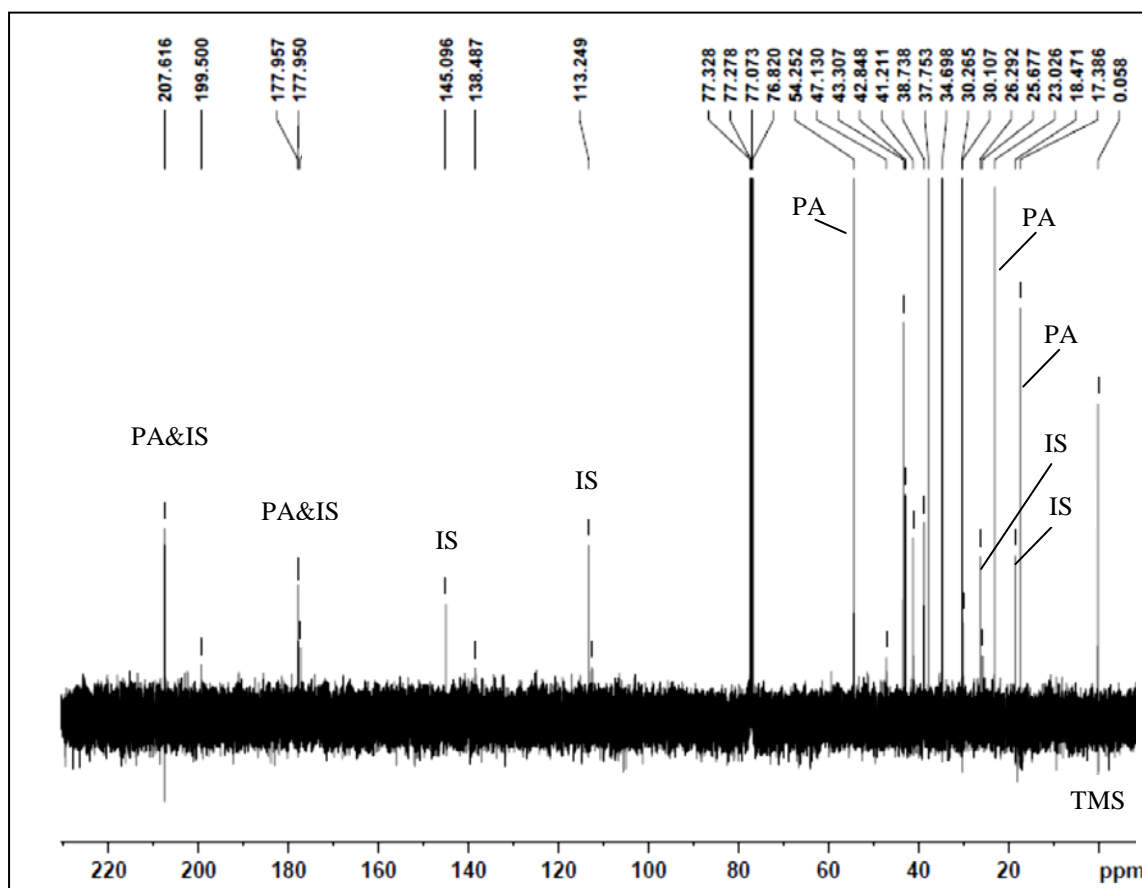


Figure S8. The ^{13}C NMR spectrum of PA after being photolyzed in chloroform- D_3 for 60 min, with most of the peaks due to PA and its isomers clearly observable. Some of the peaks are noted in the figure.

Kinetics of Aqueous-Phase Photolysis of PA

In this study we observe the progress of photolysis of PA using UV-Vis absorption spectroscopy by tracking the disappearance or appearance of absorbance at the peak of the $\pi^* \leftarrow n$ band at 280 nm. Both PA and its photolysis product(s) absorb at the observation wavelength, and we need to account for this in the analysis of data. Consider the first-order photochemical reaction, $PA \rightarrow P$ (= product), occurring with rate constant k_{PA} . The solutions for the concentrations of PA and P are:

$$\begin{aligned} [PA] &= [PA]_0 \cdot e^{-k_{PA}t} \\ [P] &= [PA]_0 \times (1 - e^{-k_{PA}t}) \end{aligned} \quad (S24)$$

The full solution would involve $[P]_0$, but it is omitted from the equation as $[P]_0=0$ in our experiments. If we assume that both PA and P can absorb radiation at the probe wavelength, and if we further assume that Beer's law holds for both species, we can write the following for the total base-10 absorbance (b = path length, and ε are molar extinction coefficients):

$$\begin{aligned} A_{10}(\lambda, t) &= b \cdot \varepsilon_{PA}(\lambda) \cdot [PA] + b \cdot \varepsilon_P(\lambda) \cdot [P] \\ A_{10}(\lambda, t) &= b \cdot \varepsilon_P(\lambda) \cdot [PA]_0 + b \cdot (\varepsilon_{PA}(\lambda) - \varepsilon_P(\lambda)) \cdot [PA]_0 \cdot e^{-k_{PA}t} \end{aligned} \quad (S25)$$

The so-called isosbestic point happens at the wavelength where the molar extinction coefficients of PA and P happen to be equal, and the time-dependent terms cancel out, which happens at $\lambda=260$ nm in our experiments (Fig. 5 in the main manuscript). The presence of the isosbestic point in the measurements lends credence to the kinetic analysis relying on the simplified $PA \rightarrow$ single product photolysis mechanism. To simplify notation, we will assume that the observation wavelength λ is 280 nm (the peak of the $\pi^* \leftarrow n$ band) and that the ratio of the molar extinction coefficients of P and PA at this wavelength is:

$$\beta = \frac{\varepsilon_P(\lambda = 280nm)}{\varepsilon_{PA}(\lambda = 280nm)} < 1 \quad (S26)$$

In addition, the initial absorbance of the solution at $t=0$ is given by:

$$A_0 = b \cdot \varepsilon_{PA}(\lambda = 280nm) \cdot [PA]_0 \quad (S27)$$

With this notation, the appropriate kinetic model for fitting the disappearance of the 280 nm absorbance by PA is:

$$A_{10}(t) = A_0 \left[\beta + (1 - \beta) \cdot e^{-k_{PA}t} \right] \quad (S28)$$

where A_0 , β , and k_{PA} are fitting constants. This is the approach taken in Fig. 4 in the main manuscript and referred to as "**Model I**".

However, as our mechanistic studies suggest, the mechanism of photolysis of PA is in fact more complicated. The primary step in the photolysis appears to produce a PA isomer (limonic acid), which also possesses a carbonyl group and can be expected to undergo secondary photolysis with a comparable rate. A more appropriate scheme to consider might be (IS = PA isomer; P = final product of photolysis):



To simplify the kinetics treatment, we will assume that the initial concentrations of IS and P are zero (this is an appropriate assumption for our experiments). In this case the rate equations and mass balance are:

$$\begin{aligned}
\frac{d[PA]}{dt} &= -k_{PA}[PA] \\
\frac{d[IS]}{dt} &= k_{PA}[PA] - k_{IS}[IS] \\
\frac{d[P]}{dt} &= k_{IS}[IS] \\
[PA]_0 &= [PA] + [IS] + [P]
\end{aligned}
\tag{S30}$$

The first-order rate constants for the PA \rightarrow IS and IS \rightarrow P steps are k_{PA} and k_{IS} , respectively. The kinetic solutions to these equations are well-known:

$$\begin{aligned}
[PA] &= [PA]_0 \cdot e^{-k_{PA}t} \\
[IS] &= \frac{k_{PA}[PA]_0}{k_{PA} - k_{IS}} \times (e^{-k_{IS}t} - e^{-k_{PA}t}) \\
[P] &= [PA]_0 \left(1 - e^{-k_{PA}t} - \frac{k_{PA}}{k_{PA} - k_{IS}} \times (e^{-k_{IS}t} - e^{-k_{PA}t}) \right)
\end{aligned}
\tag{S31}$$

For our “**Model 2**”, we can further assume that the photolysis rate constants for the PA \rightarrow IS and for IS \rightarrow P steps are roughly the same ($k = k_{PA} = k_{IS}$). This assumption is suggested by the presence of a carbonyl group in both PA and its isomer. The solution below, which was obtained by the Taylor series expansion of Eq. (S28) with respect to the difference in the photolysis rates of PA and its isomer ($k_{PA} - k_{IS}$), should be valid as long as $|k_{PA} - k_{IS}| \times t \ll 1$:

$$\begin{aligned}
[PA] &= [PA]_0 \cdot e^{-k \cdot t} \\
[IS] &\approx k[PA]_0 t e^{-k \cdot t} \\
[P] &\approx [PA]_0 (1 - e^{-k \cdot t} - k t e^{-k \cdot t})
\end{aligned}
\tag{S32}$$

Plugging this into the equation for the absorbance we get:

$$\begin{aligned}
A_{10}(\lambda, t) &= b \cdot \varepsilon_{PA}(\lambda) \cdot [PA] + b \cdot \varepsilon_{IS}(\lambda) \cdot [IS] + b \cdot \varepsilon_P(\lambda) \cdot [P] \\
A_{10}(\lambda, t) &\approx b \cdot [PA]_0 \cdot \varepsilon_P(\lambda) + b \cdot [PA]_0 (\varepsilon_{PA}(\lambda) - \varepsilon_P(\lambda) + k t \varepsilon_{IS}(\lambda) - k t \varepsilon_P(\lambda)) \times e^{-k \cdot t}
\end{aligned}
\tag{S33}$$

Once again there is a constant term and an exponentially decaying term. We will further assume that the spectrum of the isomer of PA is similar to that of PA (again, based on their structural similarity).

$$\varepsilon_{PA}(\lambda) \approx \varepsilon_{IS}(\lambda)
\tag{S34}$$

In this case, our time dependence should become:

$$A_{10}(\lambda, t) \approx b \cdot [PA]_0 \cdot \varepsilon_P(\lambda) + b \cdot [PA]_0 (\varepsilon_{PA}(\lambda) - \varepsilon_P(\lambda)) (1 + k t) e^{-k \cdot t}
\tag{S35}$$

Note that an isosbestic point is also expected in this case. However the form of the fitting equation is now different from the previously derived equation by the extra $(1+kt)$ term:

$$A_{10}(t) \approx A_0 \left[\beta + (1-\beta)(1+kt) \times e^{-k \cdot t} \right] \quad (\text{S36})$$

This equation also has 3 fitting parameters, A_0 , β , and k (same definitions as in Model 1). Attempts to fit our data to Model 2 (equation S36) resulted in poor results, suggesting that the assumptions of equal photolysis rates and equal 280 nm extinction coefficients for PA and IS are not valid.

In view of the failure of Model 2, a more realistic assumption for this particular case is that both the 280 nm molar extinction coefficient and the photolysis rate of the PA isomer are reduced by a certain constant factor ($f < 1$) relative to that of PA:

$$\begin{aligned} k_{IS} &= f \times k_{PA} \\ \varepsilon_{IS} &= f \times \varepsilon_{PA} \end{aligned} \quad (\text{S37})$$

This factor f , can be estimated from comparison of aqueous cross sections of PA (which has an absorbance-enhancing cyclobutyl ring) and acetone (which does not) as $f = 0.16$. The kinetics equations in this case become:

$$\begin{aligned} [PA] &= [PA]_0 \cdot e^{-k_{PA} \cdot t} \\ [IS] &= \frac{[PA]_0}{1-f} \times \left(e^{-f \cdot k_{PA} \cdot t} - e^{-k_{PA} \cdot t} \right) \\ [P] &= [PA]_0 \left(1 - e^{-k_{PA} \cdot t} - \frac{1}{1-f} \times \left(e^{-f \cdot k_{PA} \cdot t} - e^{-k_{PA} \cdot t} \right) \right) \end{aligned} \quad (\text{S38})$$

and the equations tracking the absorbance of the photolyzed system as a function of time at a specific wavelength become:

$$\begin{aligned} A_{10}(\lambda, t) &= b \cdot [PA]_0 \times \\ &\left[\varepsilon_{PA}(\lambda) \cdot e^{-k_{PA} \cdot t} + \frac{f \varepsilon_{PA}(\lambda)}{1-f} \times \left(e^{-f \cdot k_{PA} \cdot t} - e^{-k_{PA} \cdot t} \right) + \varepsilon_P(\lambda) \cdot \left(1 - e^{-k_{PA} \cdot t} - \frac{1}{1-f} \times \left(e^{-f \cdot k_{PA} \cdot t} - e^{-k_{PA} \cdot t} \right) \right) \right] \end{aligned} \quad (\text{S39})$$

Rearranging this gives:

$$A_{10}(\lambda, t) = b \cdot [PA]_0 \times \left[\varepsilon_P(\lambda) + \frac{(1-2f) \varepsilon_{PA}(\lambda) + f \varepsilon_P(\lambda)}{1-f} e^{-k_{PA} \cdot t} + \frac{f \varepsilon_{PA}(\lambda) - \varepsilon_P(\lambda)}{1-f} e^{-f \cdot k_{PA} \cdot t} \right] \quad (\text{S40})$$

This leads to our “**Model 3**” for the absorbance at 280 nm:

$$A_{10}(t) = A_0 \left[\beta + \frac{(1-2f) + f\beta}{1-f} e^{-k_{PA} \cdot t} + \frac{f-\beta}{1-f} e^{-f \cdot k_{PA} \cdot t} \right] \quad (\text{S41})$$

Unlike the 3-parameter models introduced above, this model has 4 fitting parameters: A_0 , β , f and k_{PA} . However, the value of f can be constrained, reducing the number of parameters back to 3.

Gas-Phase Quantum Yield Measurements Relative to Acetone

As described in the manuscript, the gas-phase photolysis rate of PAMe was obtained by observation of the decay of protonated PAMe observed with a PTR-ToF-MS instrument. An experiment with acetone, which has well-known photophysics, was conducted under identical conditions for comparison. Figure S9 shows a typical result of these measurements.

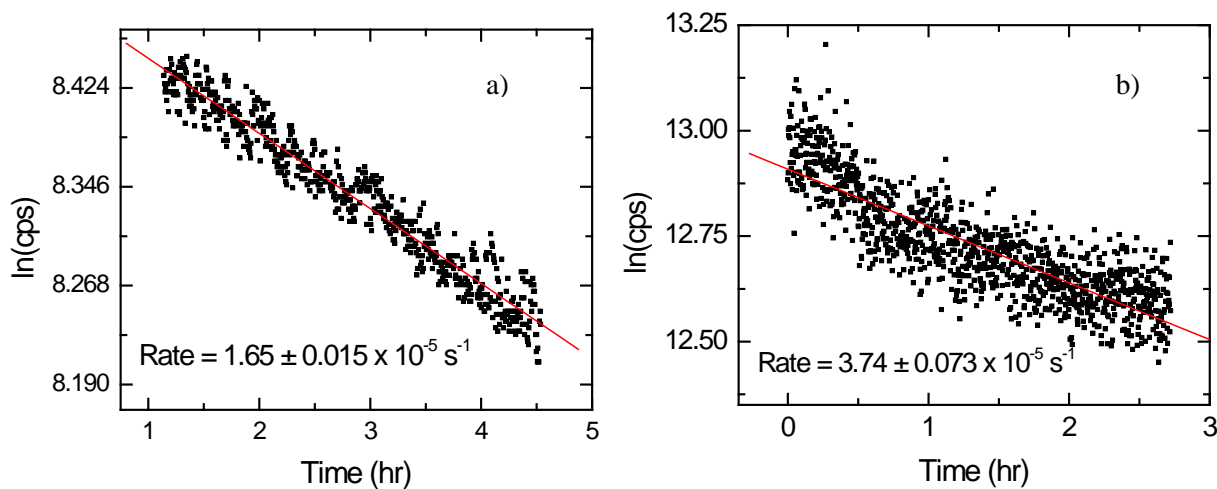


Figure S9. The decay of the PAMe signal (a) and decay of the acetone signal (b) recorded by the PTR-ToF-MS instrument under identical conditions.

Gas-Phase PAMe Photolysis Products with the PTR-ToF-MS

Figure S10 compares the high-resolution calibrated average mass spectrum taken before and after photolysis. Figure S11 shows the formation of many peaks upon photolysis. After converting the data to unit resolution, we can plot a difference spectrum comparing average measurements before and after photolysis.

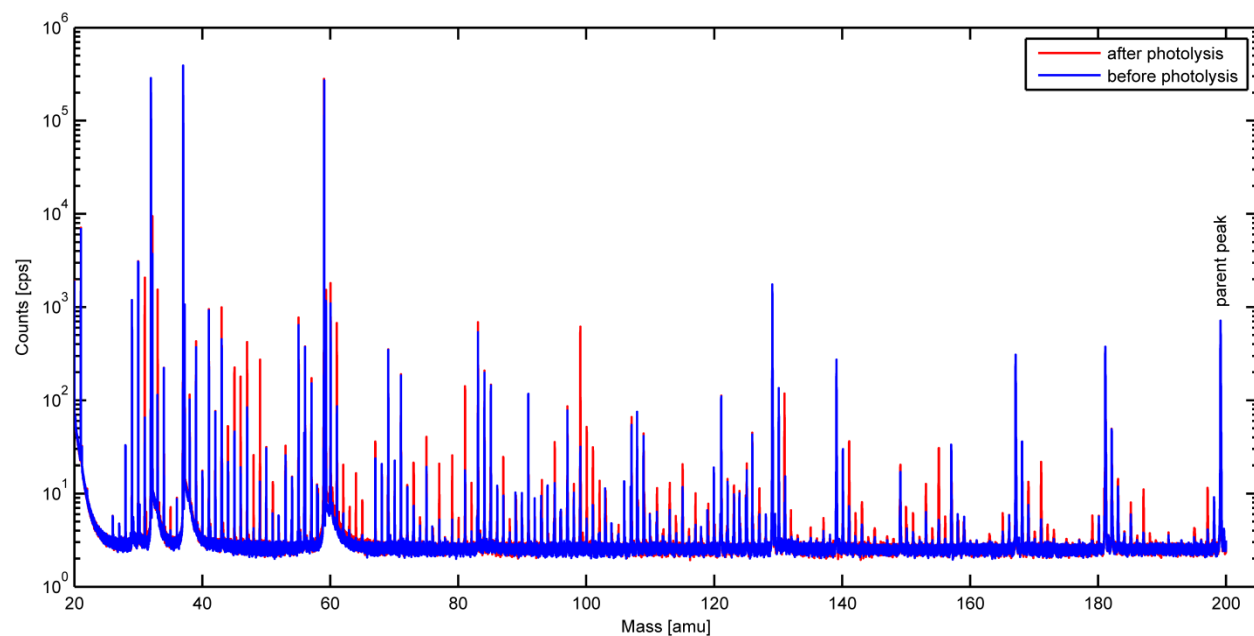


Figure S10. High-resolution PTR-ToF-MS spectrum before and after photolysis. Each spectrum is the average of 80 independent spectra. The “before photolysis” spectrum is plotted above the “after photolysis” spectrum suggesting that masses shown in red have formed during photolysis.

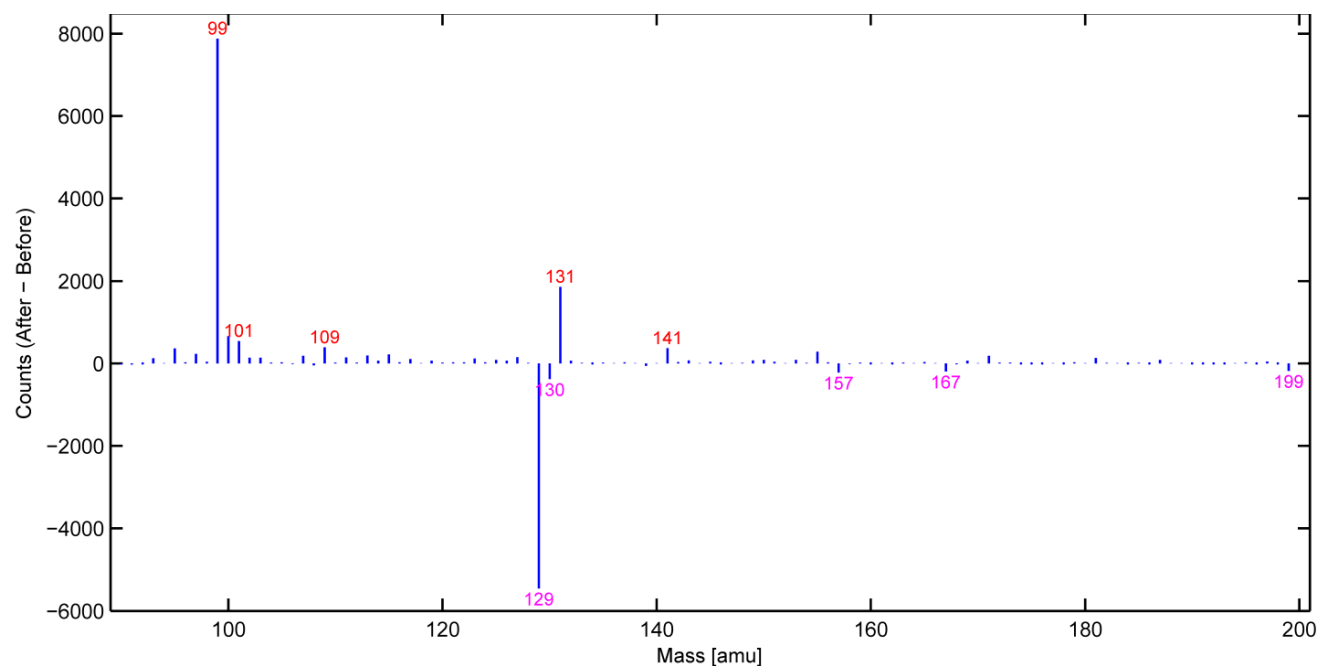


Figure S11. Unit-resolution difference spectrum comparing the counts before and after photolysis. Positive peaks indicate masses that formed upon photolysis. Negative peaks indicate masses that were consumed during photolysis.

The difference spectrum indicates that PAMe (199) was consumed and several products were formed upon photolysis. We can also track specific products identified in Schemes 2 and 3 in the manuscript as a function of photolysis time.

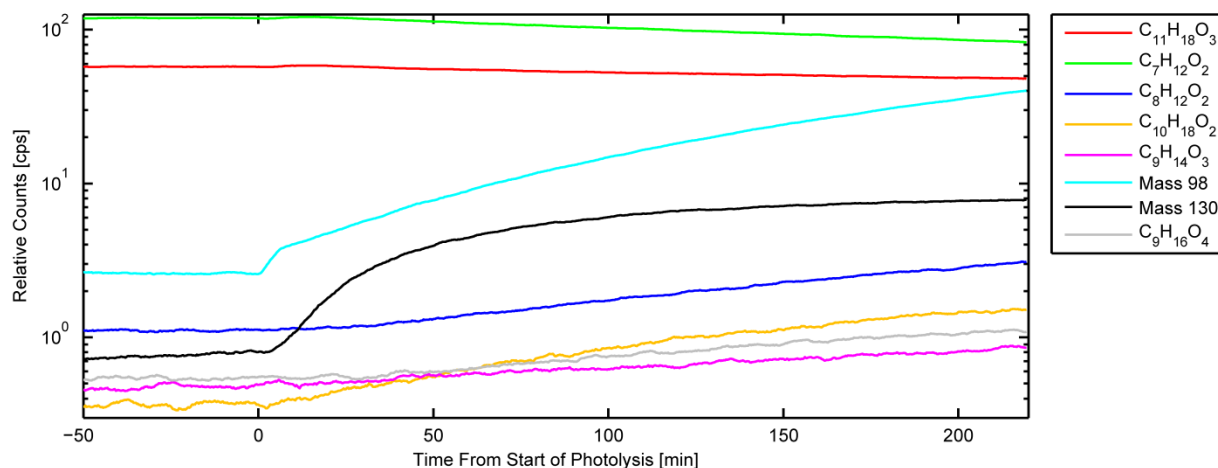


Figure S12: Relative counts as a function of photolysis time for specific products in the photolysis of PAMe. Counts are scaled by their estimated transmission, but are not corrected by the rate constants of H₃O⁺ reaction due to the absence of published data.

The C₇H₁₂O₂ signal is proportional to the PAMe (C₁₁H₁₈O₃) signal and is likely a fragment. We do not anticipate formation of Mass 98 and Mass 130 based on the chemical mechanisms. Unidentified peaks appearing at *m/z* 129.986 and *m/z* 98.0742 must come from impurities. For example, the *m/z* 129.986 peak is believed to be an impurity based on the faster time scale of its appearance compared the time scale of removal of PAMe and disappearance of other products, and also based on its negative mass defect.

Supporting Information for the Computational Section

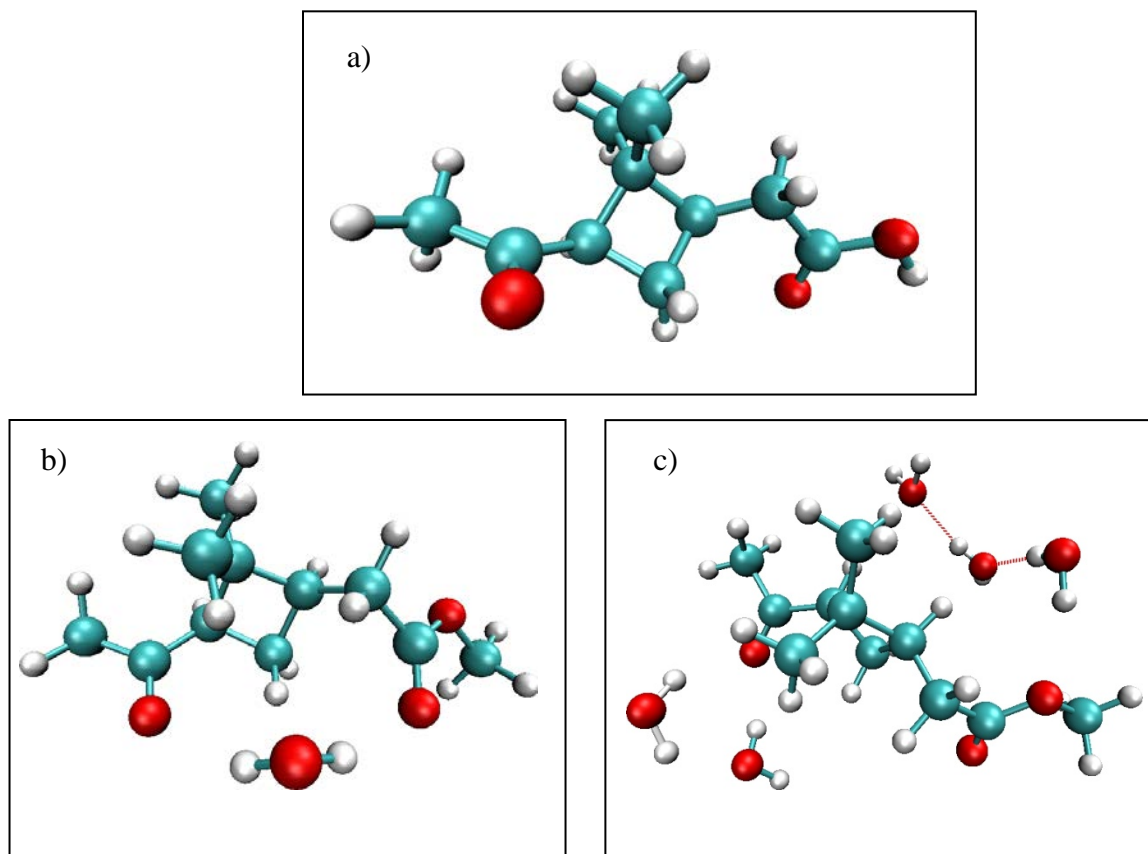


Figure S13. The optimized structures of PA and of PAMe with one water or five water molecules: a) PA, b) PAMe-H₂O, c) PAMe-(H₂O)₅. The level of theory used for predicting the structures is MP2/cc-PVDZ.

Comparison of ADC(2) and OM2/MRCI for Bare PA

Table S4. ADC(2) singlet electronic state excitation energies (ground electronic state = 0 eV). The ground state dipole is 2.91 Debye in this method.

State	Energy (eV)	Osc. Strength	Dipole (Debye)	Description
1	4.23	0.0004	1.59	HOMO -> LUMO 63 %
2	5.85	0.0005	3.25	HOMO-3 -> LUMO+2 57 %
3	7.37	0.016	5.82	HOMO -> LUMO+1 57 %
4	7.84	0.09	8.94	HOMO-2 -> LUMO 38 % HOMO -> LUMO 20 % HOMO-5 -> LUMO 14 % HOMO-1 -> LUMO 10 %

Table S5. OM2/MRCI singlet electronic state excitation energies (ground electronic state = 0 eV). The ground electronic state dipole moment is 3.73 Debye in this method.

State	Energy (eV)	Osc. Strength	Dipole (Debye)	Description
1	4.02	0.002	3.19	HOMO -> LUMO
2	5.23	0.008	4.27	HOMO-3 -> LUMO+1
3	6.53	0.03	7.17	HOMO-2 -> LUMO HOMO-1 -> LUMO
4	6.65	0.108	7.77	HOMO-2 -> LUMO HOMO-1 -> LUMO HOMO -> LUMO

Lowest Triplet State MD at 300 K for 10 and 100 ps

Table S6. Comparison of 10 ps and 100 ps MD simulations on the triplet surface for bare PA.

Events	<u>10 ps simulation</u>		<u>100 ps simulation</u>	
	Number of trajectories	Percentage	Number of trajectories	Percentage
Only vibrations	34	68 %	31	31 %
Decarboxylation	5	10 %	12	12%
4-membered ring opens	5	10 %	10	10 %
CH3-CO abstraction	5	10 %	37	37 %
H- transfer to CO group	1	2 %	10	10 %

Histograms of Time Distributions for Different Reaction Pathways

The following series of figures present the number of trajectories that react in a particular time bin. Additionally, histograms showing the number of water molecules bound to PAMe (for the PAMe-(H₂O)₅ system) at the time of the reaction are displayed.

A. Bare PA

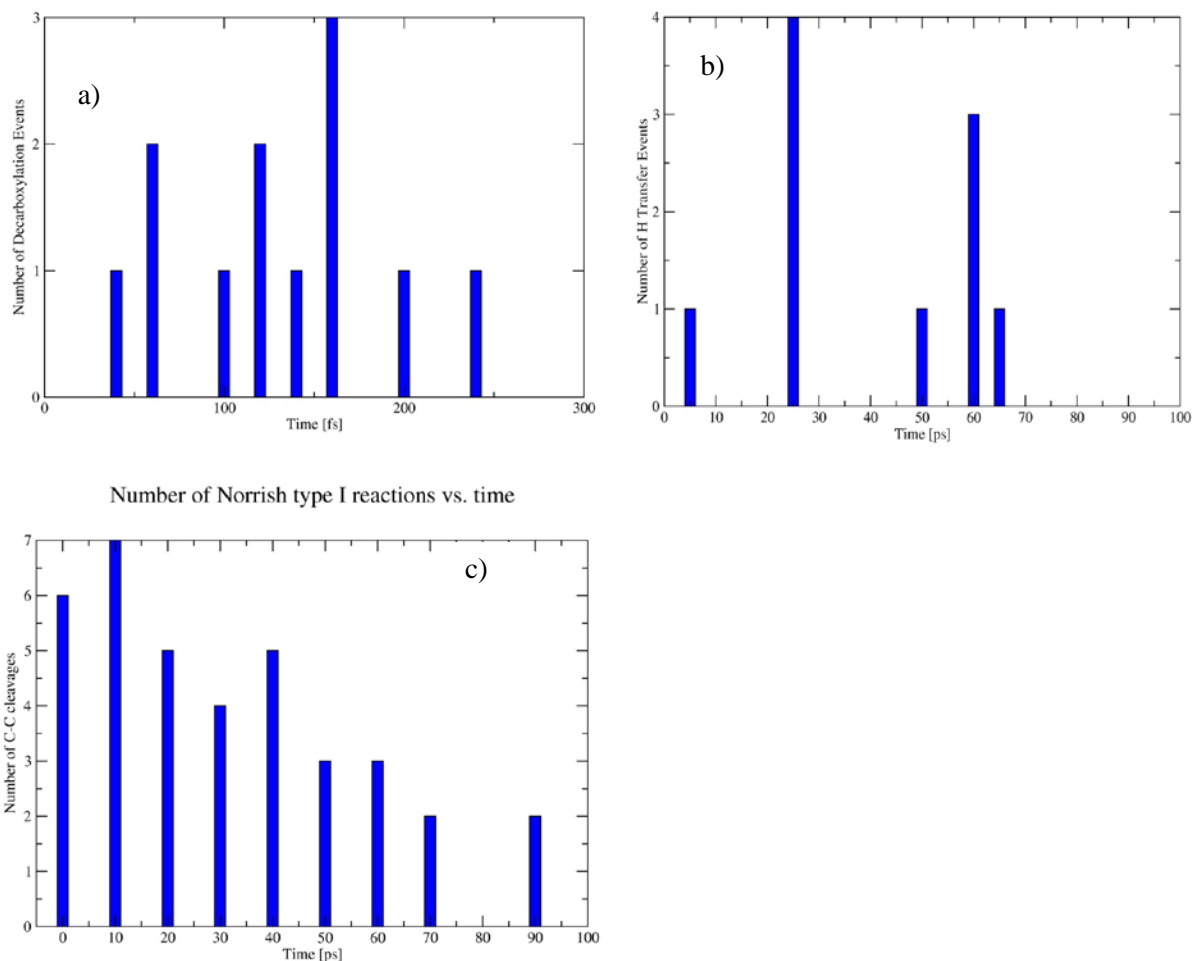


Figure S14. a) A histogram of the number of decarboxylation events found in a certain time bin. The decarboxylation takes place when the C-C distance reaches 2.5 Å. The time bin is 20 fs. b) A histogram of the number of H transfer reactions (the first step of Norrish type II reaction) in a certain time bin. The time bin is 5 ps. c) A histogram of the number of C-C cleavages (the first step of Norrish type I reaction). The time bin is 10 ps.

B. PAMe-H₂O

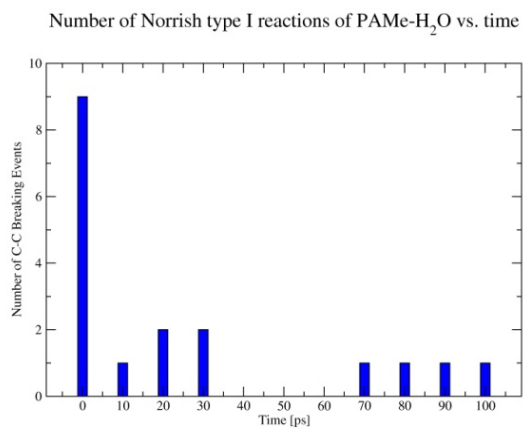
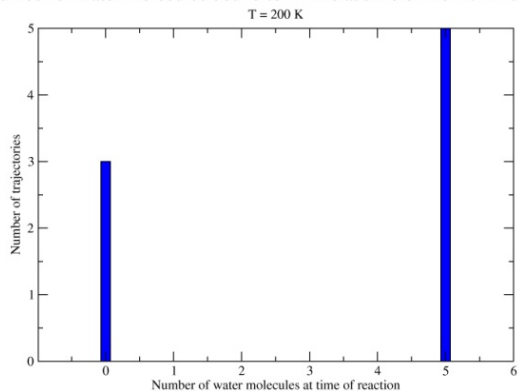


Figure S15. A histogram of the number of C-C breaking events (the first step of Norrish type I reaction). The time bin is 10 ps.

C. PAMe-(H₂O)₅

Number of water molecules bound to PAMe at time of Norrish I reaction



Number of water molecules bound to PAMe at time of Norrish II reaction

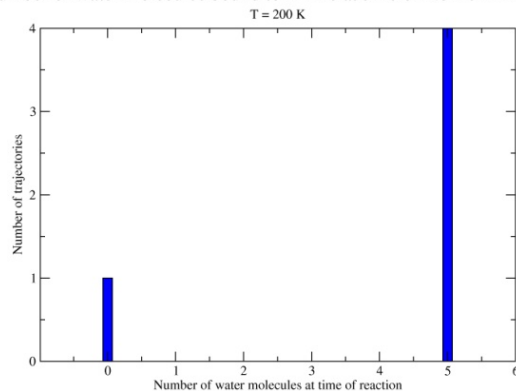
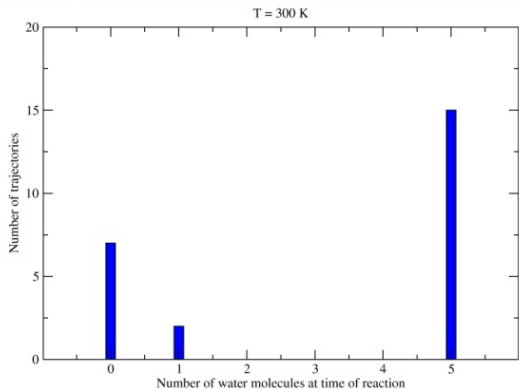


Figure S16. a) A histogram of the number of water molecules at time of Norrish type I reactions of PAMe-(H₂O)₅ at 200 K. b) A histogram of the number of water molecules at the time of Norrish type II reactions of PAMe-(H₂O)₅ at 200 K.

Number of water molecules bound to PAMe at time of Norrish I reaction



Number of water molecules bound to PAMe at time of Norrish II reaction

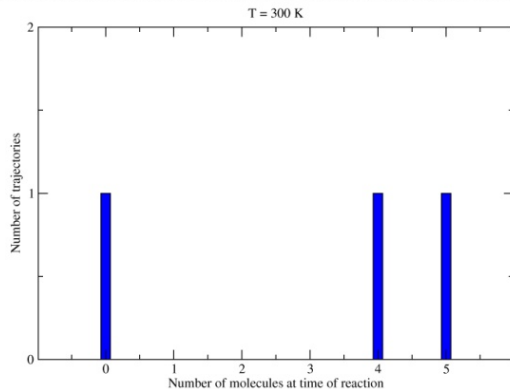


Figure S17. a) A histogram of the number of water molecules at time of Norrish type I reactions of PAMe-(H₂O)₅ at 300 K. b) A histogram of the number of water molecules at the time of Norrish type II reactions of PAMe-(H₂O)₅ at 300 K.

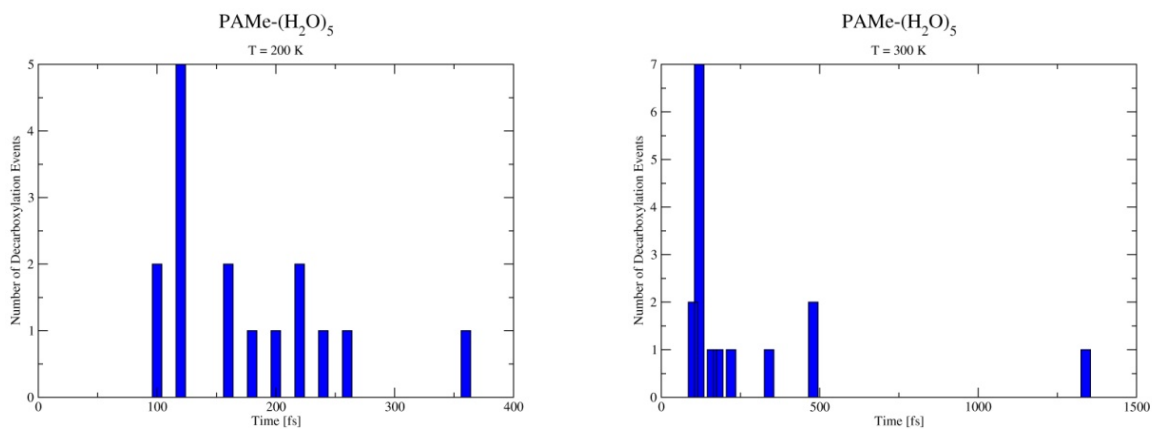


Figure S18. a) A histogram of the timescales of decarboxylation events of PAMe-(H₂O)₅ at 200 K. The time bin is 20 fs. b) Same at 300 K.

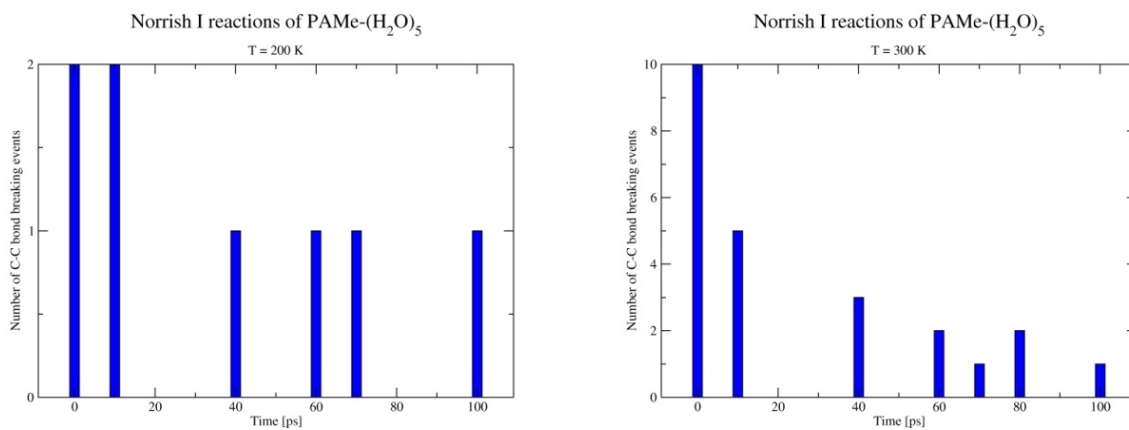


Figure S19. a) A histogram of the timescales of Norrish type I reaction of PAMe-(H₂O)₅ at 200 K. The time bin is 10 fs. b) Same at 300 K.

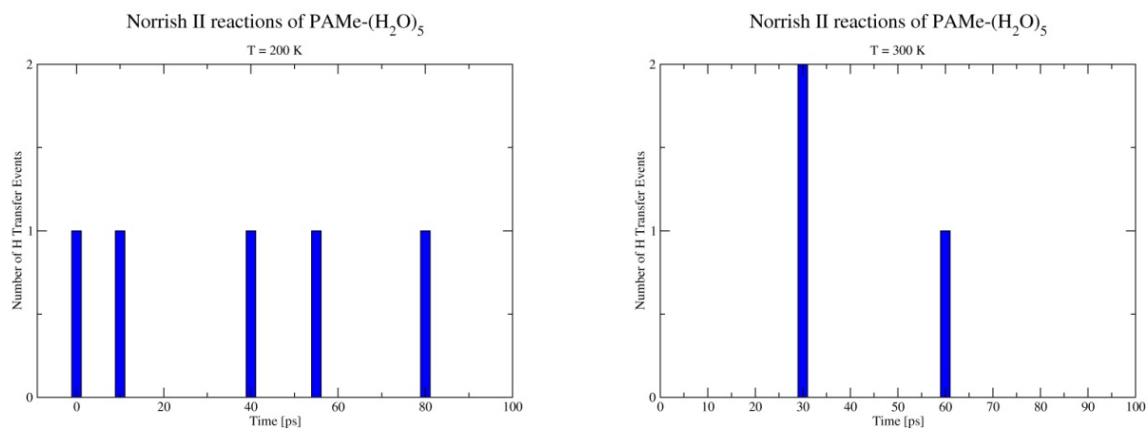


Figure S20. a) A histogram of the timescales of Norrish type II reaction of PAMe-(H₂O)₅ at 200 K. The time bin is 10 fs. b) Same at 300 K.

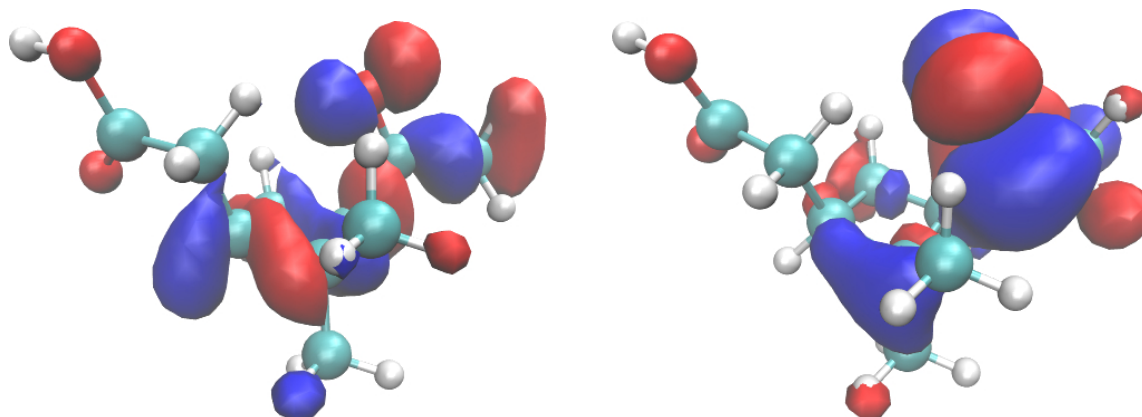


Figure S21. The HOMO (left) and LUMO (right) orbitals contributing to the S_1 electronic state of PA. Oxygen atoms are red, carbon atoms are turquoise, and hydrogen atoms are white. The excited S_1 state is a superposition of the HOMO and LUMO populated with two electrons with antiparallel spins. The excitation is mostly localized on the carbonyl group.

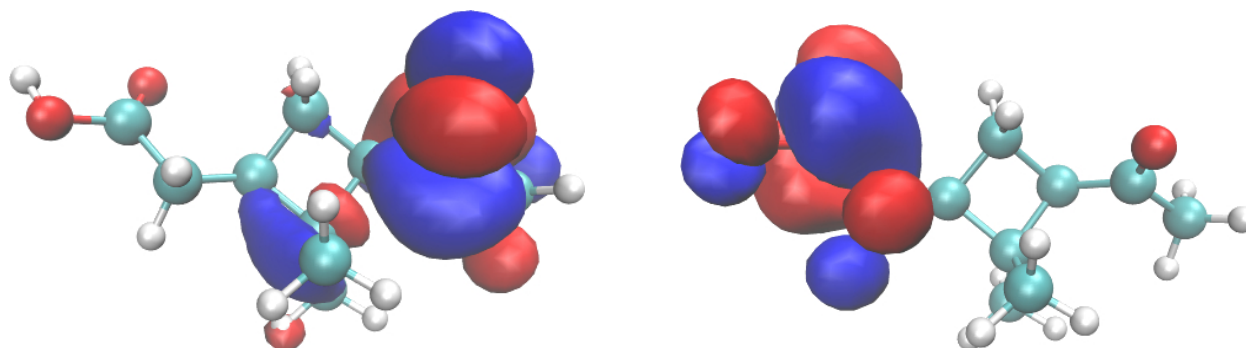


Figure S22. The HOMO (left) and LUMO (right) orbitals contributing to the T_1 electronic state of PA. Oxygen atoms are red, carbon atoms are turquoise, and hydrogen atoms are white. The excited T_1 state is a superposition of the HOMO and LUMO populated with two electrons with parallel spins. The excitation is divided between the carbonyl and carboxyl groups.